

Rapid immunosurveillance by recirculating lymphocytes in the rat intestine: critical role of unsulfated sialyl-Lewis X on high endothelial venules of the Peyer's patches

Tomomi Uchida^{1*}, Hisashi Ueta^{1*}, Xue-Dong Xu², Jotaro Hirakawa³, Kazunori Tahara⁴,
Shu Zhou⁵, Yasushi Sawanobori¹, Szandor Simmons⁶, Yusuke Kitazawa¹, Hiroto Kawashima³
and Kenjiro Matsuno¹

¹Department of Anatomy (Macro), Dokkyo Medical University, School of Medicine, Tochigi 321-0293, Japan

²Department of General Surgery, Dalian Medical University, 1st Affiliated Hospital, Dalian 116011, China

³Laboratory of Microbiology and Molecular Genetics, Graduate School of Pharmaceutical Sciences, Chiba University, Chiba 260-8675, Japan

⁴Division of Surgery, Department of Surgical Specialties, National Center for Child Health and Development, Tokyo 157-8535, Japan

⁵Department of Gynecology, Dalian Medical University, 1st Affiliated Hospital, Dalian 116011, China

⁶Department of Immunology and Cell Biology, Graduate School of Medicine and Frontier Biosciences and WPI-Immunology Frontier Research Center, Osaka University, Osaka 565-0871, Japan

Correspondence to: H. Ueta; E-mail: ueta@dokkyomed.ac.jp

*These authors equally contributed to this work.

Received 25 September 2017, editorial decision 12 December 2017; accepted 03 January 2018

Abstract

Naive lymphocytes systemically recirculate for immunosurveillance inspecting foreign antigens and pathogens in the body. Trafficking behavior such as the migration pathway and transit time within the gastrointestinal tract, however, remains to be elucidated. Rat thoracic duct lymphocytes (TDLs) were transferred to a congenic host that had undergone mesenteric lymphadenectomy. The migration pathway was investigated using newly developed four-color immunohistochemistry and immunofluorescence. Donor TDLs showed rapid transition in gut tissues from which they emerged in mesenteric lymph around 4 h after intravenous injection. Immunohistochemistry showed that donor TDLs predominantly transmigrated across high endothelial venules (HEVs) at the interfollicular area of the Peyer's patches (PPs), then exited into the LYVE-1⁺ efferent lymphatics, that were close to the venules. The rapid recirculation depended largely on the local expression of unsulfated sialyl-Lewis X on these venules where putative dendritic cells (DCs) were associated underneath. Recruited naive T cells briefly made contact with resident DCs before exiting to the lymphatics in the steady state. In some transplant settings, however, the T cells retained contact with DCs and were sensitized and differentiated into activated T cells. In conclusion, we directly demonstrated that lymphocyte recirculation within the gut is a very rapid process. The interfollicular area of PPs functions as a strategically central site for rapid immunosurveillance where HEVs, efferent lymphatics and resident DCs converge. PPs can, however, generate alloreactive T cells, leading to exacerbation of graft-versus-host disease or gut allograft rejection.

Keywords: alloresponse, blood-lymph transition, dendritic cells, lymphatics, T cells

Introduction

All immune cells constantly monitor for the intrusion of harmful factors as a way to maintain organismal homeostasis. To respond systemically to local inflammatory stimuli,

lymphocytes successively patrol tissues, known as recirculation, entering from the blood vessels, scanning the tissue and then exiting to the lymphatics (1). A large number of non-self

factors, such as food antigens, ions and sometimes harmful pathogens, are ordinarily internalized through the absorptive epithelium of the intestine. The intestines are equipped with the highest number of immune cells, mostly resident innate cells and migratory lymphocytes (2). What remains unclear, however, are the specifics of the trafficking of recirculating lymphocytes to the intestine, including aspects related to the migration pathway, dwell time within the tissue and relevant molecules. Previously, we reported the migration kinetics and routes of recirculating lymphocytes in the rat liver (3). Their kinetics involve a rapid process in which the transit time of recruited lymphocytes is 4–6 h at steady state. This rapid transit may enable an efficient surveillance of the liver by the recirculating lymphocytes.

In this study, we first estimated the transit time of recirculating lymphocytes in the intestine by directly counting gut-derived cells in the mesenteric lymph. Second, we traced the migration route in the gut tissue using a newly developed four-color immunohistochemistry approach and then identified relevant molecules crucial for the lymphocyte trafficking. Finally, we addressed the significance of these findings in terms of homeostatic immunosurveillance as well as pathogenesis of transplant immunity in the gut.

Methods

Animals

Inbred PvG/c (RT1.A^cB^c), Lewis (RT1.A^B) and DA (RT1.A^aB^a) rats were supplied by SLC Co. (Shizuoka, Japan). Congenic PvG-RT.7^b/OlaHsd rats (RT1.A^cB^c, RT.7^b) and (PvG/c x Lewis) F₁ hybrid rats (RT1.A^dB^d) were bred and maintained in the laboratory Animal Research Center (Dokkyo Medical University). All animals were reared under specific pathogen-free conditions. Animal handling and care was approved by the Dokkyo Medical University Committee, and in accordance with the Dokkyo University's Regulations for Animal Experiments and with Japanese Government Law (No. 105). Congenic PvG-RT.7^b male rats were used as donors, unless otherwise specified. General anesthesia was used for surgery, and euthanasia. Anesthesia was administered using isoflurane (Mylan Inc., Tokyo, Japan), given with an isoflurane vaporizer (SN-487-OT, Shinano Manufacturing, Tokyo, Japan).

Antibodies and reagents

Mouse hybridoma cells against the congenic marker RT.7^b, clone HIS41, were kindly donated by Dr F. G. M. Kroese (Groningen University, the Netherlands). Monoclonal antibodies (mAbs), polyclonal antibodies (pAbs), labeled secondary antibodies and substrates used are listed in [Supplementary Table S1](#) (available at [International Immunology Online](#)). Some mAbs were purified from culture supernatants and coupled to FITC, biotin (Dojindo, Kumamoto, Japan) and Alexa Flour conjugates (Thermo Fisher Scientific) in house.

Experimental design

In the first experiment, the intestinal blood-lymph transit assay, the transit time of gut-derived recirculating lymphocytes was estimated by counting the number of donor cells

in the thoracic duct lymph of recipient rats that had undergone mesenteric lymphadenectomy (MLNx) 6 weeks earlier, which resulted in the direct influx of the gut lymph into the thoracic duct after regeneration of the lymphatics (Fig. 1A). In the second experiment, multicolor immunohistochemistry or immunofluorescence was performed to analyze the spatiotemporal distribution of donor cells in the intestinal tissue. We also explored the molecules involved in the rapid

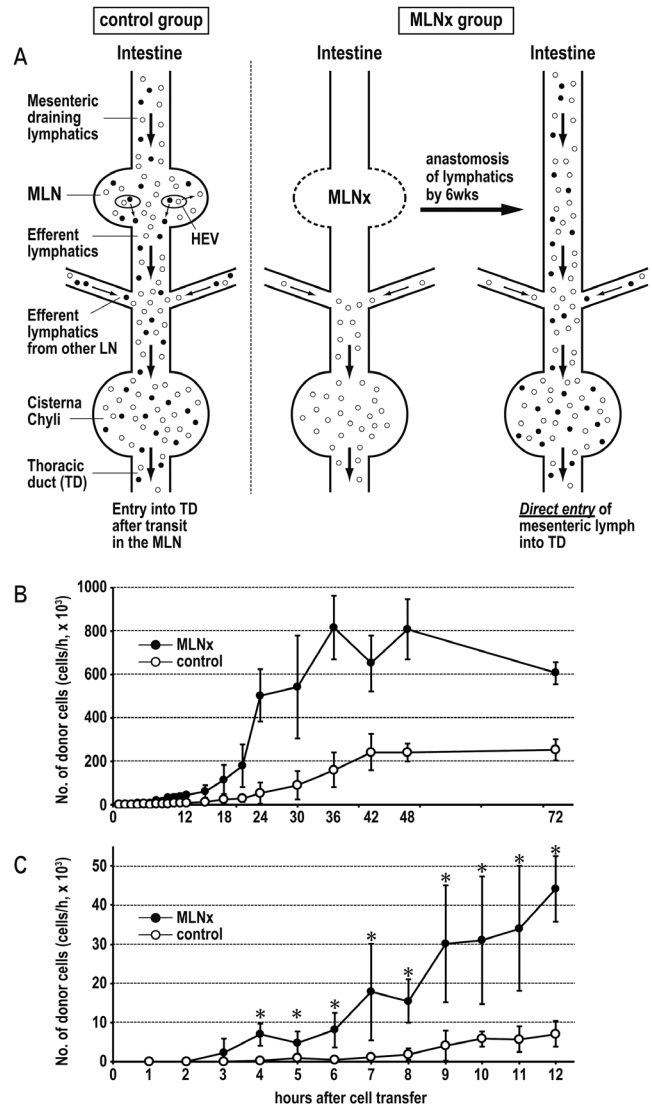


Fig. 1. Kinetics of recirculating lymphocytes in rat intestine. (A) Schematic summary of lymphocyte trafficking in the MLNx group and control group. In the MLNx group, congenic donor lymphocytes (filled circle) from intestine directly flowed into the thoracic duct without being trapped in the MLN. Open circles indicate host lymphocytes. (B, C) Intestinal blood-lymph transit assay: time kinetics of total donor cell output in the thoracic duct lymph in the MLNx group and control group. An early-stage variant of (B) is more precisely shown in (C). (B) More donor recirculating lymphocytes appeared in the MLNx group (filled circle) than in the control group (closed circle) through the experiment. (C) An early time scale (~12 h) of (B). Donor cell output in the MLNx group was significantly increased at 4 h after transfer. Each bar in (B) and (C) represents means \pm SD ($n = 5$). * $P < 0.05$, versus control group.

blood-lymph transition in the gut in an immunohistological study of gut endothelium, flow cytometry of donor lymphocytes and an *in vivo* short-homing and blood-lymph transit assay with anti-selectin ligand antibody. Finally, we focused on T-cell behavior in the Peyer's patches (PPs), especially an interaction with tissue dendritic cells (DCs) in terms of immunosurveillance at steady state and their significance in transplant immunity.

Animal studies

MLNx of 5- to 7-week-old PvG/c rats was performed as described previously, with minor modification (3). The rats were allowed to recover more than 6 weeks to ensure anastomosis of the afferent and efferent lymphatics of the excised nodes (Fig. 1A). The thoracic duct lymphocytes (TDLs) of PvG-RT.7^o rats were obtained by routine thoracic duct cannulation and were collected aseptically overnight at 4°C. The TDLs were labeled with 10 μ M CFSE (Thermo Fisher Scientific) for 20 min at 37°C. The viability of labeled TDLs was consistently >95% as assessed by the trypan blue dye exclusion method. A total of 1×10^8 cells per rat of TDLs were injected intravenously (i.v.) into host PvG/c rats that had received thoracic duct cannulation immediately before cell transfer.

In the intestinal blood-lymph transit assay, thoracic duct lymph was collected every hour up to 12 h, then at 15, 18, 21, 24, 30, 36, 42, 48 and 72 h after transfer. To avoid imposing great stress, the subject rats were cared for dedicatedly during cannulation. An actual body weight (BW) loss after 72-h cannulation was $13.4 \pm 2.4\%$ ($n = 6$), which was much less than those of wasting conditions such as in rats developing acute graft-versus-host disease (GvHD), where their BW rapidly dropped >30% in 3 days (4). After counting the hourly output of total lymphocytes, cytospot smears were prepared. The proportion of CFSE⁺ cells to total cells for each cytospot smear was counted under a fluorescent microscope with a differential interference contrast aid (Axioskop2 plus, Carl Zeiss, Jena, Germany), and the total donor cell output per hour was calculated. In some cases, the host PvG/c rat was injected i.v. with 1 mg of anti-sialyl-Lewis X mAb, F2 1 h before congenic TDL transfer. Donor TDLs in thoracic duct lymph were counted and analyzed by FACS.

In the short-homing assay, donor TDLs were prepared from PvG-RT.7^o male rats by thoracic duct cannulation as above. After two washes with PBS, 1×10^8 cells were i.v. transferred to congenic PvG/c rats that 1 h before had received F2 mAb (500 μ g per rat). Two hours after the donor cell transfer, single cell suspensions were prepared from the host PPs, small intestines and peripheral lymph nodes (LNs), and the proportion of donor cells was determined by FACS.

Rat small intestinal transplantation was performed orthotopically between allogenic (DA rat to Lewis rat) or syngenic (Lewis rat to Lewis rat) combinations as previously described (5).

Immunohistological analysis

To analyze the spatiotemporal distribution of donor lymphocytes in the gut tissue, double or triple immunohistochemistry was performed as described previously (6). In brief, tissues

were embedded in Tissue-Teck O.C.T. compound (Sakura Finetek, Tokyo, Japan) and fresh cryosections 4 μ m thick prepared. For labeling proliferating cells, rats received an i.v. injection of BrdU (6 mg per 200 g body weight, for immunohistochemistry) or equivalent moles of 5-ethynyl-2'-deoxyuridine (EdU) (for immunofluorescence (7)) in sterile PBS 1 h before sacrifice. Immunofluorescent images were captured by a fluorescent microscope equipped with an AxioCam MRm camera (Carl Zeiss). To depict the tissue framework more clearly, original blue images from type IV collagen staining were converted to pseudocolor white with Axiovision software (Carl Zeiss). To quantitatively analyze the positional relationship between MHCII cells and MAdCAM-1⁺ high endothelial venules (HEVs) with or without F2 antigen, the sub-endothelial zone was defined as a continuous belt with 10- μ m width in the peripheral margin of the basement membrane of the MAdCAM-1⁺ HEV by Axiovision software, and then the number of MHCII⁺ cells inside this zone was counted. In some cases, fluorescent images were captured by the confocal laser microscopy LSM780 (Carl Zeiss).

For analyzing the *in situ* kinetics of donor cells in detail, donor cells and multiple tissue components and/or interacting cells were simultaneously visualized in the same section by newly established four-color immunohistochemistry. We first incubated a cocktail of antibodies consisting of a biotinylated mAb against recipient class II MHC (MHC-II), anti-LYVE1 pAb and a fluorescein-conjugated mAb against anti-congenetic marker (HIS41). After three washes with PBS, streptavidin-conjugated β -galactosidase (β -gal) was incubated then light blue color was developed by using X-gal (Tokyo Chemical Industry Co. Ltd, Tokyo, Japan) as a substrate for β -gal. Sequential incubation with enzyme-linked secondary antibody followed by the substrate reaction was performed step by step, which resulted in red (NewFuchsin, Dako, Carpinteria, CA, USA) and blue (Vector Blue, VECTOR, Burlingame, CA, USA) staining for lymphatics and donor lymphocytes, respectively. As a last step, the tissue framework was stained with anti-type IV collagen pAb and visualized in brown with diaminobenzidine. In some cases, biotinylated anti-MAdCAM-1 mAb was used instead, followed by streptavidin-conjugated peroxidase. Black color was developed by using ImmPACTTM SG (VECTOR) as a substrate. Enzyme inhibition was conducted after color development when the same enzyme-substrate system was used at a later step. A schematic of the protocol is shown in [Supplementary Figure S1](#) (available at *International Immunology Online*).

Flow cytometry

Cervical LNs, mesenteric LNs, the PPs and intestinal tract without the PPs were aseptically excised and then incubated with Liberase TM (Roche Diagnostics, Indianapolis, IN, USA) for 5 min at 37°C. Before enzymatic digestion, the PPs and gut were pretreated for 30 min at 37°C with stirring in EDTA solution to remove mucus. After quenching the enzyme digestion by further incubating for 5 min with 5 mM EDTA, the cell suspension was washed three times with PBS containing 2 mM EDTA, 5% FCS and 100 μ g ml⁻¹ DNase I (Roche). After Fc γ II receptor blocking (BD Bioscience, Franklin Lakes, NJ, USA), the cells were stained with fluorochrome-conjugated antibodies. Stained

cells were acquired on an Attune NxT flow cytometer (Thermo Fisher Scientific Inc.) or FACSCalibur (BD Biosciences) and data were analyzed with FlowJo ver. 9.2 (FlowJo LLC, Ashland, OR, USA). T cells and B cells were defined as TCR $\alpha\beta$ ⁺B220⁻ and TCR $\alpha\beta$ ⁻B220⁺ cells, respectively.

Statistical analysis

Statistical analysis was performed using the Student's *t*-test.

Results

Kinetics of recirculating lymphocytes from the intestine

In the MLNx group, recirculating lymphocytes that had egressed from the intestine could directly enter the thoracic duct lymph without being trapped in the regional LNs of the intestine, the MLN (Fig. 1A). In the intestinal blood-lymph transit assay, donor cells appeared in the thoracic duct lymph more rapidly in the MLNx group when compared with controls (Fig. 1B). Of note, the donor cell emergence in the thoracic duct lymph was significantly higher at 4 h after cell transfer in the MLNx group (Fig. 1C).

PPs as the rapid blood-lymph transition site in the intestine

Immunohistology of intestinal tissue 3 h after congenic lymphocyte transfer revealed that the cells were distributed predominantly at the interfollicular areas of the PPs (Fig. 2A–C). In FACS analysis for donor cells in the intestinal tissue, about 7×10^6 of donor cells migrated to the PPs, whereas a negligible number of cells did so to the small and large intestine (Fig. 2D). Thus, these studies suggested that donor lymphocytes preferentially entered gut tissues from HEVs in the PPs.

Next, we investigated the expression of MAdCAM-1 (mucosal addressin cell adhesion molecule-1) on blood vessels and the vasculature of LYVE-1⁺ lymphatics in the gut tissues. Triple immunohistochemistry showed that MAdCAM-1⁺ venules as well as LYVE-1⁺ lymphatics were distributed both in the interfollicular area of the PPs and in the lamina propria of intestinal villi. It should be noted that these vasculatures run side by side in close proximity (Fig. 2E–G) in the gut tissues. To analyze the interrelationship between donor cells and these vessels in the PPs, four-color immunohistochemistry was newly developed in which donor cells, MAdCAM-1⁺ HEV and LYVE-1⁺ lymphatics were visualized simultaneously using brightfield microscopy (Fig. 2H, J–L). At 3 h after transfer, donor lymphocytes that had transmigrated across the MAdCAM-1⁺ HEV were readily found near to LYVE-1⁺ lymphatics at the interfollicular area (Fig. 2J and K) and some had begun to egress into LYVE-1⁺ vessels (Fig. 2H, I and L). This cellular kinetics was consistent with the appearance of gut-derived donor cells in the thoracic duct lymph of the MLNx group at 4 h after cell transfer (Fig. 1C).

Site-specific expression of unsulfated sialyl-Lewis X in MAdCAM-1⁺ blood vessels in the intestine and its role for lymphocyte trafficking

To clarify the mechanisms for the preferential homing for donor lymphocytes to the PPs, we examined the expression of cell migration-associated molecules in both lymphocytes and

blood vessels in the gut. FACS analysis showed that although transferred donor T and B cells were strongly positive for L-selectin, they were weakly positive for $\beta 7$ integrin and negative for CCR9, which are involved in the selective migration for gut-homing lymphocytes (Fig. 3A) (8). Immunohistochemical analysis for their corresponding ligands in the gut tissues showed uniform expression of ICAM-1, P-selectin (both not shown) and MAdCAM-1 (Fig. 2E–G) on vascular endothelial cells of HEVs in the PPs and venules in the intestinal villi. In contrast, 6-sulfo sialyl-Lewis X (6-sulfo sLe^x), known as a major ligand for L-selectin and recognized by S2 mAb in the peripheral LNs (9), was expressed on neither the PP HEVs (Fig. 3B and C) nor venules in the intestinal villi (not shown). Of note, the vessels in the PPs, but not in the villi, were selectively stained with another recently developed mAb, F2, which reacts with the *N*-acetyl and *N*-glycolyl forms of sLe^x structure (Fig. 3C) (10), in a PP-dependent manner (Fig. 3D–I).

We then examined the role of F2 glycotope in lymphocyte trafficking to the gut tissue by a short-term homing assay. With F2 pretreatment, migration of donor lymphocytes at 2 h after transfer was significantly suppressed not only in the peripheral LNs but also in the PPs when compared to isotype IgG (Fig. 3J). Donor cells in the villus lamina propria of the small intestine were rather slightly increased by the F2 pretreatment, but not statistically significantly (Fig. 3J). Furthermore, in the intestinal blood-lymph transit assay with MLNx rats, donor cell emergence in thoracic duct lymph was significantly inhibited by F2 pretreatment, when compared with non-pretreated MLNx rats (Fig. 3K and L). Control studies, in which normal mouse IgG1, an isotype IgG of F2 mAb, did not affect *per se* both transmigration of donor TDLs to host secondary lymphoid organs and the output of recirculating lymphocytes in the thoracic duct lymph (Supplementary Figure 2, available at *International Immunology* Online). These results confirm the validity of the inhibitory effect of F2 mAb in this assay. Of note, fluorescent immunohistochemistry revealed that the expression of the F2 glycotope was observed in the MAdCAM-1⁺ HEVs at the interfollicular area (Fig. 4A). Four-color immunofluorescence further revealed that unsulfated sLe^x was selectively expressed at MAdCAM-1⁺ HEVs where MHC-II⁺ cells with dendritic morphology were significantly accumulated underneath (Fig. 4B–I).

Rapid recirculation of naive T cells via PPs and its significance in immunosurveillance and transplantation immunity

FACS analysis for donor cells in the migration site revealed that >60% of migrant cells in the peripheral LNs were T cells as in the original TDLs, while B cells were dominant in the PPs at 2 h after cell transfer (Fig. 5A). However, the donor cell type in the thoracic duct lymph that had egressed from MLNx-treated gut up to 6 h post-transfer was exclusively T-cell dominant (Fig. 5A). Sphingosin-1-phosphate receptor, which is involved in T-cell exit from tissue to lymphatics, was expressed to the same degree in donor T cells in the PPs when compared with those of peripheral LNs (Fig. 5B). Four-color immunohistochemistry of the PPs, 3 h post-transfer, showed that many donor lymphocytes in the interfollicular area made contact with MHC-II⁺ cells with dendritic morphology, and some of the donors had already entered the lymphatics (Fig.

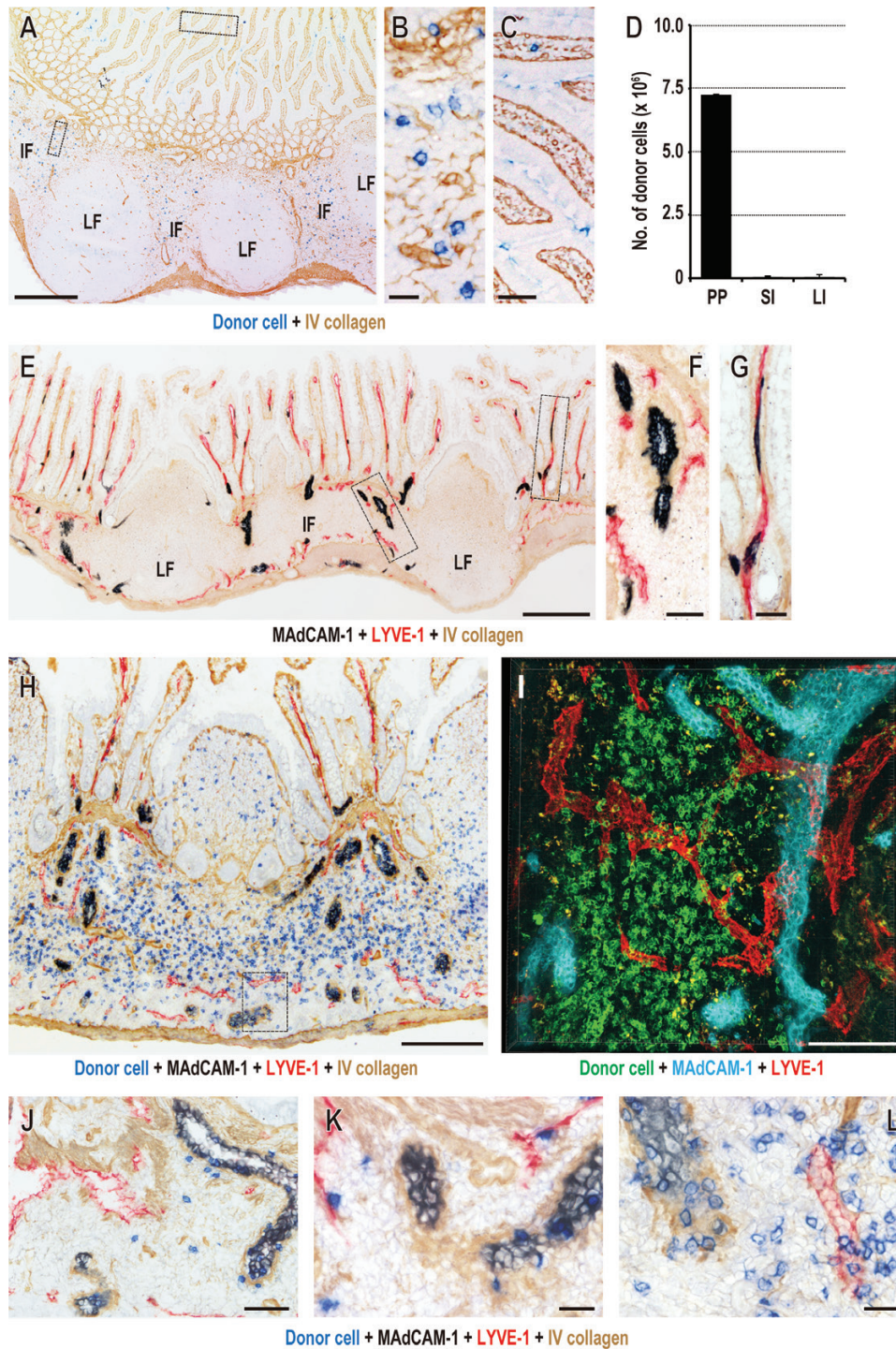


Fig. 2. Naive lymphocytes recirculate the gut by transiting at PPs. (A–C) Donor cell distribution in the host intestinal tissue 2 h after transfer; double stained with congenic donor cells (blue) and type IV collagen (brown). (B, C) Interfollicular area (B) and lamina propria (C) encircled in dotted lines in (A). (D) Total number of donor cells in the tissue 2 h after transfer (1×10^8 cells). SI, small intestine; LI, large intestine. (E–G) Triple staining of MadCAM-1 (black), LYVE-1 (red) and type IV collagen (brown). (F, G) Interfollicular area and villus lamina propria encircled in dotted lines in (E). (H, I, K, L) Four-color immunohistochemistry for donor cells (blue), MadCAM-1 (black), LYVE-1 (red) and type IV collagen (brown) at 0.5 h (J), 2 h (K) and 3 h (H, L; encircled area in (H)) after donor TDL transfer (5×10^8 cells). Note some donor cells in the LYVE-1⁺ lymphatics at 3 h (L). (I) Three-dimensional aspects of donor cells (green), MadCAM-1 (light blue) and LYVE-1 (red) at the interfollicular area of PPs 3 h after donor cell transfer (5×10^8 cells). IF, interfollicular area; LF, lymph follicle. Scale bars: (A) 400 μ m; (B) 20 μ m; (C) 50 μ m; (E) 300 μ m; (F, G) 50 μ m; (H) 200 μ m; (I) 100 μ m; (J) 50 μ m; (K, L) 20 μ m.

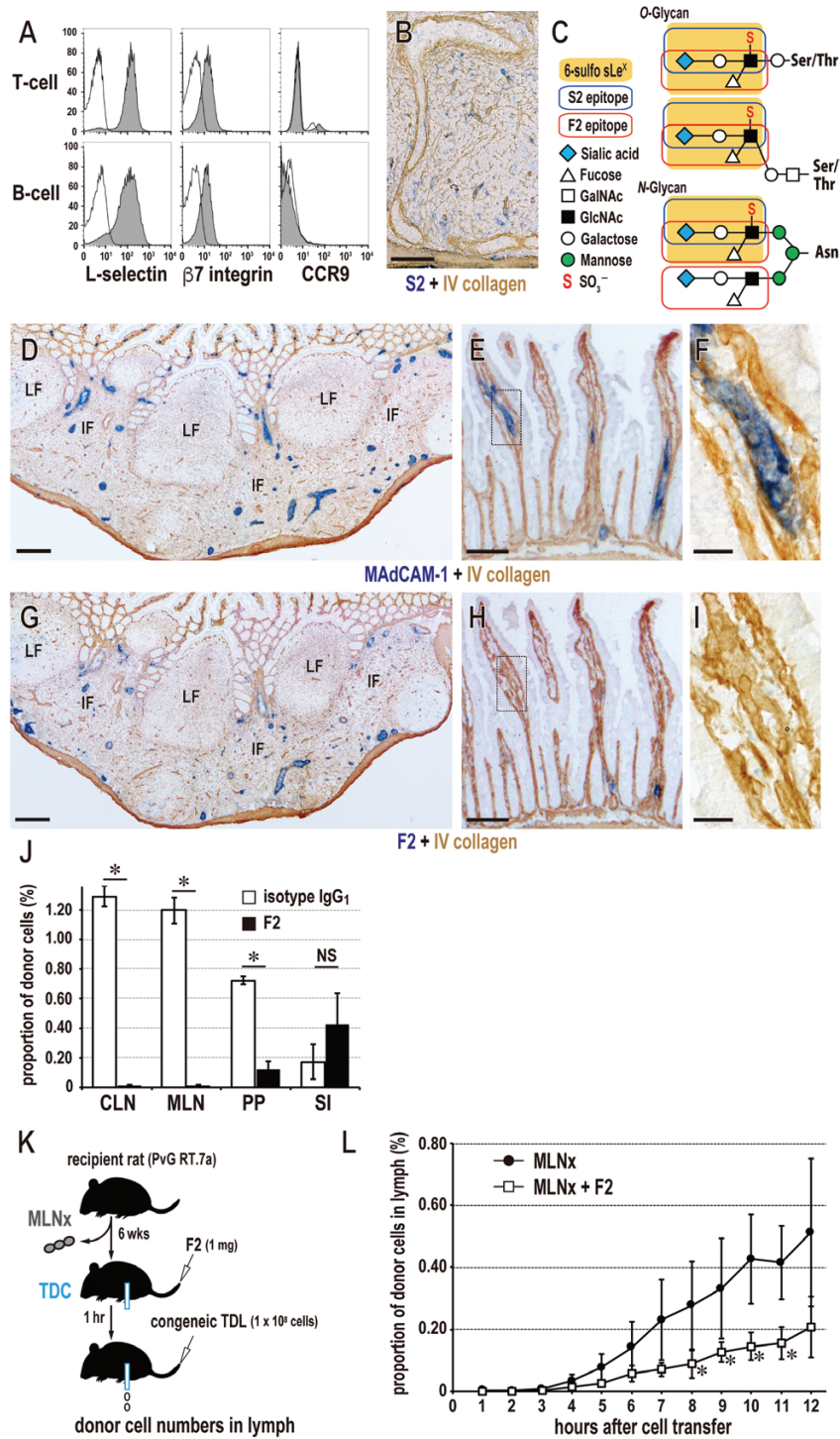


Fig. 3. Local expression of unsulfated sialyl-Lewis X and its role in lymphocyte recirculation. (A) Expression of gut-homing molecules (filled histogram) on naive T cells and B cells. Open histogram: isotype control. (B) Double staining of S2 and type IV collagen in the interfollicular area of PPs. (C) Structures of O- and N-glycans modified with the 6-sulfo sialyl-Lewis X moiety, and recognition determinants S2 and F2. (D–I) Double staining for MadCAM-1 (blue, D–F) or F2 (blue, G–I) and type IV collagen in the PPs (D, G) or intestinal villi (E, F, H and I). (F, I) Inset of (E) and (H), respectively. (J) Short-homing assay. Donor TDLs (1×10^8 cells) were injected intravenously into a host rat that had received 0.5 mg of F2 1 h before. Two hours after cell transfer, CFSE⁺ donor cells in single cell suspensions from target tissues were quantified by FACS. * $P < 0.01$, versus control group. (K) Scheme of inhibition assay for lymphocyte blood-lymph transition by F2. (L) Kinetics of donor cell proportion in the host thoracic duct lymph. CFSE⁺ donor cells in thoracic duct lymph cells collected hourly were quantified by FACS. Note a significant decrease in donor cell proportion in the F2-treated group (open square) compared with control group (filled circle). * $P < 0.05$, versus control group. IF, interfollicular area; LF, lymph follicle. Scale bars: (B) 100 μ m; (D, G) 200 μ m; (E, H) 100 μ m; (F, I) 20 μ m. Each bar in (J) and (L) represents means \pm SD ($n = 3$).

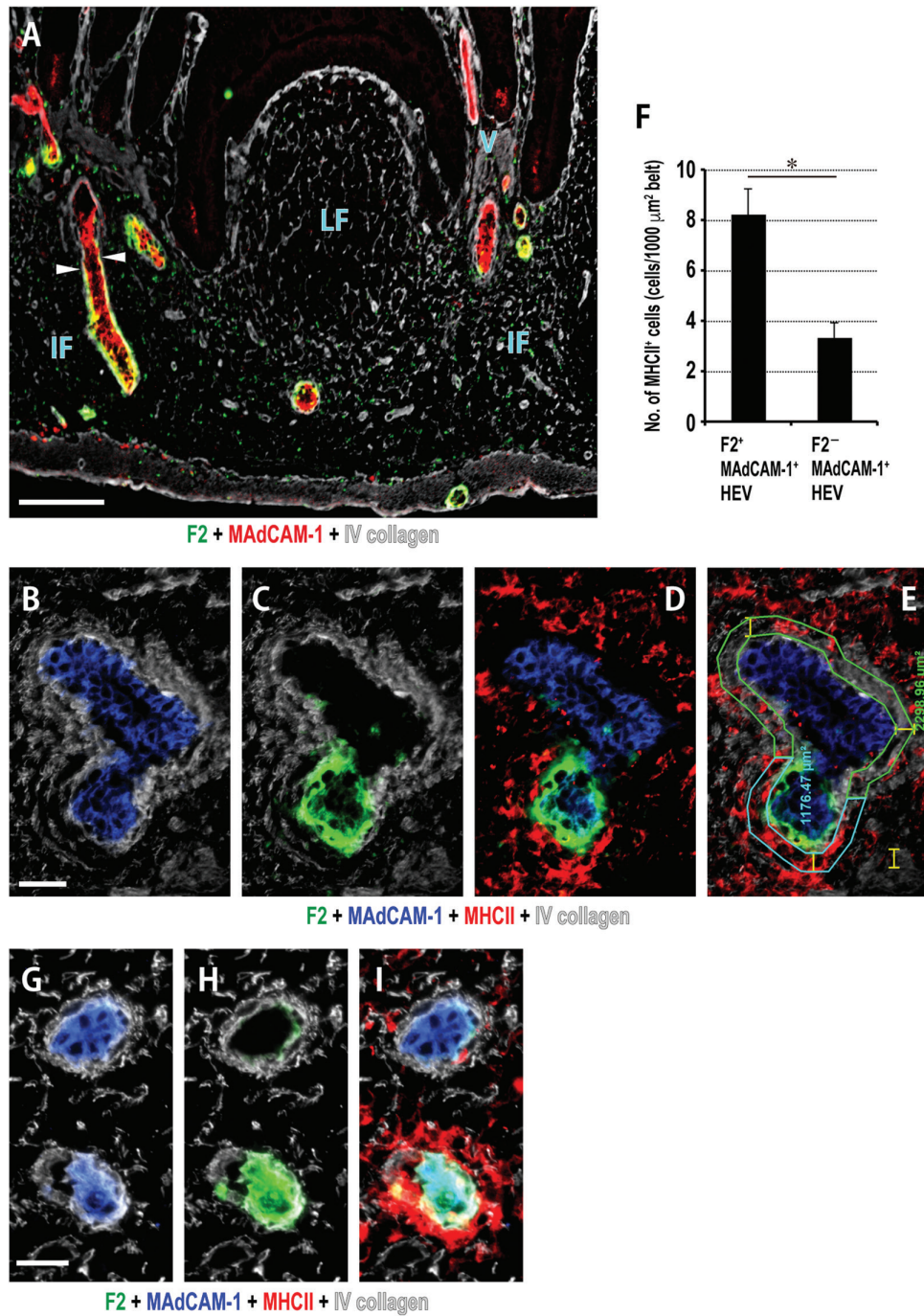


Fig. 4. Area-specific expression of F2 glycoepitope on MAdCAM-1⁺ HEVs. (A) Four-color immunofluorescence for F2 (green), MAdCAM-1 (red), MHC-II (purple) and type IV collagen (gray) in the PPs. Note that F2 glycoepitope was started to express at the IF area (arrowhead) but not the V area. (B–E) Four-color immunofluorescence at the boundary area of F2 glycoepitope expression. Note that local expression of F2 (green) on MAdCAM-1⁺ HEVs (blue) where MHC-II⁺ cells (red) accumulating underneath the vessels (D). (E) Defining the sub-endothelial zone, and (F) Number of MHC-II⁺ cells in the sub-endothelial zone. Note F2 glycoepitope was predominantly expressed on MAdCAM-1⁺ HEVs where more than four MHC-II⁺ cells distributed in 1000 μm^2 of sub-endothelial zone surrounding HEVs. Bar indicates mean \pm SD ($n = 3$). $P < 0.01$. (G–I) Same horizontal section of MAdCAM-1⁺ HEVs at interfollicular area. Yellow bar in (E) 10 μm ; (B–D) 20 μm .

5C and D). These results suggested that migrated T cells first contacted with the PP DCs, forming a cellular cluster at the interfollicular area to inspect antigens presented by DCs; if not, they soon detached from the cluster and departed into lymphatics nearby to restart circulation at the steady state.

In contrast, when donor T cells were transferred to a semi-allogenic recipient, they similarly entered the intestinal tissue and made contact with the PP DCs as well (Fig. 5E). Some of them became BrdU⁺ large lymphoblasts within the cluster (Fig. 5F). The number of proliferating cells at the interfollicular

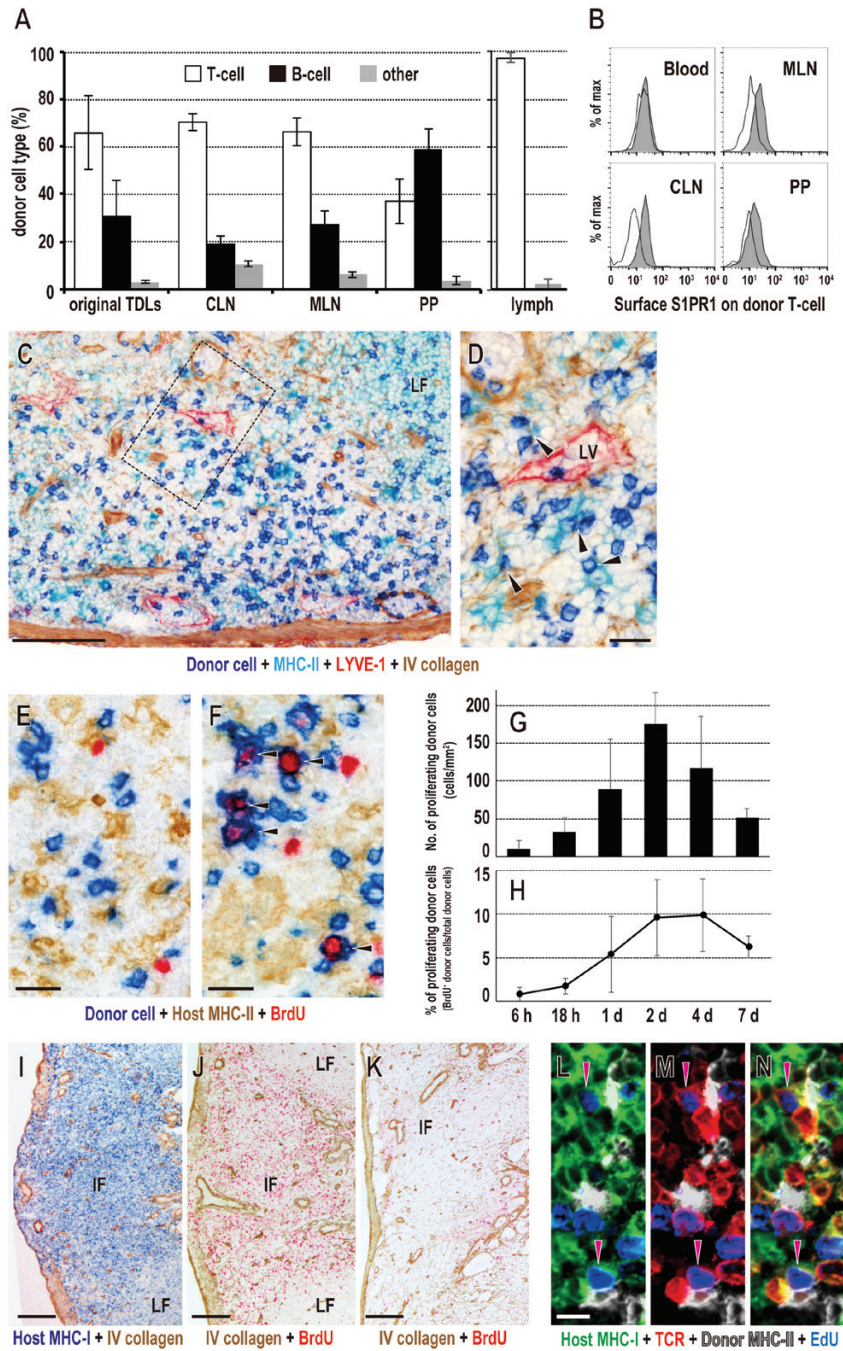


Fig. 5. Rapid recirculation of naive T cells in the PPs and the clinical significance for transplant immunity. (A) Proportions of a lymphocyte subset were analyzed in original donor TDLs, from donor cells in the single cell suspension from each host lymphoid organ 2 h after donor cell transfer, and from thoracic duct lymph up to 6 h by FACS. (B) Expression of Sphingosin-1-phosphate receptor (filled histogram) on donor T cells in the PPs 3 h after cell transfer. Open histogram: isotype control. CLN, cervical LN. (C, D) Four-color immunohistochemistry for donor cells (blue), MHC-II (light blue), LYVE-1 (red) and type IV collagen (brown). Note that some donor cells are contacting MHC-II cells in the interfollicular area (arrowhead in (D)). (D) Inset of (C). (E–H) Fate of donor T cell in the allogeneic PPs. Donor T cells that contacted with MHC-II⁺ cells and reside in the host PPs were originally small and round cells at 3 h after transfer (E), but some became proliferating large lymphoblasts at day 3 (arrowheads (F)). (G, H) Kinetics of the proliferative response of donor cells. (G) The number of donor proliferating cells/mm², (H) the proportion of proliferating donor cells. (I–N) Fate of host T cells in the donor PPs after small intestinal transplantation. (I) Graft PPs were immediately occupied by host MHC-I⁺ cells at day 2 after transplantation. (J, K) Massive proliferative responses at the interfollicular area in allogeneic graft (J), but not in syngeneic graft (K) at day 2. (L–N) Four-color immunofluorescence for host MHC-I (green), T-cell receptor $\alpha\beta$ (red), donor MHC-II (white) and EdU (blue). Note that host MHC-I⁺TCR $\alpha\beta$ ⁺ T cells became enlarged and proliferated with forming of the cell cluster with donor MHC-II⁺ cells (purple arrowheads in (N)). Day 2 after transplantation. IF, interfollicular area; LF, lymph follicle; LV, lymphatic vessel; S1PR1, Sphingosin-1-receptor 1; EdU, 5-ethynil-2'-deoxyuridine. Scale bars: (C) 100 μ m; (D) 20 μ m; (E, F) 20 μ m; (I–K) 200 μ m; (L–N) 10 μ m. Each bar in (A, G and H) represents means \pm SD ($n = 3$).

area was largely increased at day 2 (Fig. 5G), and ~10% of total donor cells were proliferating from days 2 to 4 (Fig. 5H).

In addition, in the allotransplantation settings of the small intestine, where a part of the donor intestinal tract including the PPs was transplanted to the host, graft PPs were subjected to enormous numbers of infiltrating host cells and were occupied by host MHC-I cells at day 2 (Fig. 5I). Also, vigorous proliferative responses were observed exclusively at the interfollicular area of the graft PPs when compared with those of the syngenic graft (Fig. 5J and K). Recently established four-color immunofluorescent microscopy using EdU (7) clearly showed that most of the proliferating cells were host MHC-I⁺TCR $\alpha\beta$ ⁺ T cells, which directly contacted with donor MHC-II⁺ cells at day 2 thereafter (Fig. 5L–N). These activated T cell–DC clusters may represent a site of the direct pathway of allosensitization as reported previously (11, 12).

Discussion

In this study, we directly showed the transition time of recirculating lymphocytes in the intestine by counting transferred cells in the mesenteric lymph of congenic host rats that had been subjected to MLNx. The estimated minimal transit time was 4 h after i.v. transfer, which is very rapid similar to that of the liver (3) but shorter than that of the peripheral LNs (13). Using multicolor immunohistochemistry, we clearly demonstrated the close proximity of MAdCAM-1⁺ HEVs to LYVE-1⁺ lymphatics in the gut tissue. A previous report involving scanning electron microscopic observation of corrosion casts in rabbit PPs suggested a close association of lymphatics with HEVs (14). This association was also observed in mice (S. Simmons, unpublished data), suggesting that the close apposition of HEVs with the lymphatics is conserved across animal species at least in the PPs. These anatomical features would enable the migrated lymphocytes to exit more rapidly in starting recirculation.

Previous studies indicated that a predominant distribution of donor cells in the interfollicular area of the PPs and few cells in the small and large intestine (15). In this study, we confirmed these observations quantitatively by FACS, indicating that the PPs are the major site for intestinal blood-lymph transition in a steady state. In this respect, immunohistochemistry also revealed that MAdCAM-1⁺ HEVs express a unique type of L-selectin ligand in a PP-specific manner, as discussed below. Research involving intravital microscopy in rats has indicated that fluorochrome-labeled lymphocytes migrate into microlymphatics of the PPs, which were assigned by drainage of pre-injected vital dyes at 240 min after transfer (16). These results may support our findings. Antigen sampling in the small intestine has largely been performed in a specialized compartment of the PPs, the follicle-associated epithelium rather than the villus epithelium (17). In addition, although intestinal DCs constantly migrate to draining LN, MLN where they present cognate antigen to naive T cells, their turnover rate is much slower than that of naive lymphocytes (18, 19). Thus, in terms of defense against incoming pathogens and toxins landing at the mucous surface of the body, it would be strategically reasonable to selectively recruit naive lymphocytes at the PPs where foreign antigens are preferentially incorporated in order to survey them quickly and efficiently.

It is well known that modifications of HEV peripheral node addressin (PNAd), such as sialylation and fucosylation, are indispensable for L-selectin⁺ lymphocyte homing across the HEVs. Sulfation of sLe^x is also important for effective homing to the peripheral LNs: however, lymphocyte migration toward the PPs is not impaired in knockout mice lacking sulfotransferases (GlcNAcST-1 and 2) (20). Recent transcriptomic analysis of mice HEVs showed that expression of the HEV-specific sulfotransferase, GlcNAcST-2 is less than 10-fold lower in the PPs than in the peripheral LNs (21). In addition, the S2 mAb, which recognizes the 6-sulfo sLe^x structure, does not inhibit lymphocyte homing to mice PPs, although it reacts with PP HEV *in situ* (10). These results suggested a minor role of sulfation in the PP HEV homing in mice. In the present study, the rat PPs were not stained with S2 at all but stained with F2 instead. F2 recognizes the sLe^x moiety on O- and N-glycan regardless of sulfation while S2 recognizes only the sulfated form (Fig. 3C), suggesting that sLe^x on the rat PP HEVs should be unsulfated. The significant block of lymphocyte homing to the PPs and the delayed donor cell appearance in the mesenteric lymph (Fig. 3K and M) by F2 mAb indicated that unsulfated sLe^x did play a critical role in the rapid transition of recirculating lymphocytes in the PPs. On the other hand, in agreement with the abovementioned mouse study (10), lymphocyte homing partly persisted in rat PPs when compared with other LNs by F2 pretreatment (Fig. 3J). The residual migrants after F2 pre-treatment were not only B cells but also T cells (H. Ueta, unpublished data), suggesting the presence of selectin-independent homing abilities in each cell type, such as CD22-mediated B-cell homing (22) and the involvement of MAdCAM-1:α4β7 integrin interaction, which compensates for the weaker avidity between lymphocyte L-selectin and unsulfated sLe^x on the PP HEVs when compared with 6-sulfo sLe^x (20). Also, this axis might be involved in naive lymphocyte homing to the intestinal lamina propria.

It is noteworthy that in gut tissues, unsulfated sLe^x was expressed exclusively in the MAdCAM-1⁺ HEVs in the interfollicular area (Fig. 3J). According to a recent review of HEVs, MAdCAM-1⁺ immature HEVs develop into MAdCAM-1⁺PNAd⁺ cuboidal mature HEVs by non-canonical NF-κB signaling driven by continuous stimulation with lymphotoxin-β receptor on HEVs (23). CD11c⁺ DCs are thought to be among the candidates for lymphotoxin-providing cells and depletion of CD11c⁺ cells in CD11c-DTR transgenic mice results in the loss of PNAd expression and inhibition of lymphocyte recruitment (24). In our multicolor immunohistological study, some PP DCs were distributed in the vicinity of and made contact with MAdCAM-1⁺F2⁺ HEVs (Fig. 4). Therefore, local unsulfated sLe^x expression may represent functional maturation of the HEVs, which might be regulated by a distinct type of DC subset located at the interfollicular area of the PPs (25).

Also of interest is that the cell types of recirculating lymphocytes in the PPs 2 h after transfer were relatively B-cell dominant, while those of mesenteric lymph up to 6 h were almost all T cells (Fig. 5A). Therefore, homeostatic naive T-cell kinetics are very fast; immediately after transmigrating HEVs, they formed cell clusters with resident DCs, and then rushed into neighboring lymphatics at steady state. Blast formation followed by transient proliferative response of T cells in an allogeneic host (Fig. 5F–H) suggested that the PPs act not only as a blood-lymph transition site but also

as a major site of immunoactivation for naive T cells when encountering the cognate antigen presented by DCs, as well as spleen and peripheral LNs (26, 27). In other words, the PPs could be an essential site in generating alloreactive T cells in the transplant setting. Indeed, it was proposed in a mouse model of acute GvHD that donor naive T cells differentiated to effector cells in the PPs and that the disease did not develop in the PP-deficient host (28).

Furthermore, in the case of small intestinal transplantation, an enormous number of host T cells would quickly flood into the graft PPs soon after re-vascularization and make contact with donor resident DCs within the graft (Fig. 5I, J, L–N). This mode of interaction is a direct host-versus-graft reaction (HvGR), where host naive T cells developed into anti-donor effector T cells because of direct sensitization by donor DCs, leading to graft rejection (11, 29). Of note, unlike liver transplantation where intra-graft proliferative responses are prominent around day 4 after transplantation (11, 29), much more severe BrdU responses were induced even at day 2 at the interfollicular area of the graft PPs in the current work (Fig. 5J). In terms of sensitization site, alloreactive host T cells against the hepatic allograft are mainly generated at host secondary lymphoid organs by 'intra-host' direct HvGR where passenger donor DC migration is a prerequisite (11), while those of intestine are generated within the graft by 'intra-graft' direct HvGR. Thus, effector T cells from the latter would soon exert their cytotoxicity without trafficking and accumulate stronger damage against the graft. Preoperative donor DC depletion along with HEV blockade by each antibody *ex vivo* (4) might be an effective manipulation for preventing intra-graft sensitization and prolonging graft survival. Taken together, as a mucosa-associated lymphoid tissue, the PPs are equipped with specialized structures that enable rapid transition and antigen presentation to naive T cells for effective immunosurveillance at steady state. However, these features also contribute to serious complications involving transplant immunity.

Methodologically, although immunofluorescence staining is useful for analyzing multiple parameters, it is difficult to gain a complete observation of the signals through the tissue in the dark field. In this study, we newly established four-color immunohistochemistry in which the particular cells, vessels and tissue framework were simultaneously visualized using brightfield (Supplementary Figure S1, available at *International Immunology Online*). The result was high visibility and made it possible to understand more deeply and precisely the positional relationship among migrated lymphocytes, HEVs and lymphatics in the PPs. This method would be applicable for other detailed analysis for *in situ* multicellular interactions in other investigations.

Conclusion

In conclusion, we directly demonstrated that lymphocyte recirculation within the gut is a rapid process comparable to that of LN and liver. Four-color immunohistochemistry revealed that PPs function as a strategically central site for rapid immunosurveillance and recirculation for T cells where unsulfated sLe^x-positive HEVs, efferent lymphatics and resident DCs converge. However, the PPs also may provide the opportunity to generate alloreactive T cells which can lead to complications for transplantation therapy.

Supplementary data

Supplementary data are available at *International Immunology Online*.

Funding

This study was partly supported by Dokkyo Medical University Young Investigator Award (2015-10 to T.U.), Dokkyo Medical University Project Research Grant (2012-02-1 to H.U.) and JSPS KAKENHI Grant Number (JP17K08518 to K.M.).

Acknowledgements

We are grateful to Drs F. G. M. Kroese, H. Kimura and professor T. B. Issekutz for generously providing hybridoma cells against RT.7^b, RT1.A¹ and $\beta 7$ integrin, respectively. The authors also are grateful for the excellent technical support and advice provided by Il-Y. Hwang, K. Sasaki and Y. Yamada. We also appreciate professors K. Toida and E. Kiyokage for valuable discussions and comments.

Conflicts of interest statement: the authors declared no conflicts of interest.

References

- Butcher, E. C. and Picker, L. J. 1996. Lymphocyte homing and homeostasis. *Science* 272:60.
- Mowat, A. M. and Agace, W. W. 2014. Regional specialization within the intestinal immune system. *Nat. Rev. Immunol.* 14:667.
- Xu, X. D., Ueta, H., Zhou, S. *et al.* 2008. Trafficking of recirculating lymphocytes in the rat liver: rapid transmigration into the portal area and then to the hepatic lymph. *Liver Int.* 28:319.
- Yu, E., Ueta, H., Kimura, H., Kitazawa, Y., Sawanobori, Y. and Matsuno, K. 2017. Graft-versus-host disease following liver transplantation: development of a high-incidence rat model and a selective prevention method. *Am. J. Transplant.* 17:979.
- Schwarz, N. T., Nakao, A., Nalesnik, M. A., Kalf, J. C., Murase, N. and Bauer, A. J. 2002. Protective effects of *ex vivo* graft radiation and tacrolimus on syngeneic transplanted rat small bowel motility. *Surgery* 131:413.
- Kariya, T., Ueta, H., Xu, X. D. *et al.* 2016. Direct evidence for activated CD8⁺ T cell transmigration across portal vein endothelial cells in liver graft rejection. *J. Gastroenterol.* 51:985.
- Kitazawa, Y., Ueta, H., Hünig, T., Sawanobori, Y. and Matsuno, K. 2015. A novel multicolor immunostaining method using ethynyl deoxyuridine for analysis of *in situ* immunoproliferative response. *Histochem. Cell Biol.* 144:195.
- Iwata, M., Hirakiyama, A., Eshima, Y., Kagechika, H., Kato, C. and Song, S. Y. 2004. Retinoic acid imprints gut-homing specificity on T cells. *Immunity* 21:527.
- Hirakawa, J., Tsuboi, K., Sato, K. *et al.* 2010. Novel anti-carbohydrate antibodies reveal the cooperative function of sulfated N- and O-glycans in lymphocyte homing. *J. Biol. Chem.* 285:40864.
- Matsumura, R., Hirakawa, J., Sato, K. *et al.* 2015. Novel antibodies reactive with sialyl Lewis X in both humans and mice define its critical role in leukocyte trafficking and contact hypersensitivity responses. *J. Biol. Chem.* 290:15313.
- Ueta, H., Shi, C., Miyanari, N. *et al.* 2008. Systemic transmigration of allosensitizing donor dendritic cells to host secondary lymphoid organs after rat liver transplantation. *Hepatology* 47:1352.
- Saiki, T., Ezaki, T., Ogawa, M., Maeda, K., Yagita, H. and Matsuno, K. 2001. *In vivo* roles of donor and host dendritic cells in allogeneic immune response: cluster formation with host proliferating T cells. *J. Leukoc. Biol.* 69:705.
- Tomura, M., Yoshida, N., Tanaka, J. *et al.* 2008. Monitoring cellular movement *in vivo* with photoconvertible fluorescence protein "Kaede" transgenic mice. *Proc. Natl Acad. Sci. USA* 105:10871.
- Ohtani, O. and Murakami, T. 1990. Organization of the lymphatic vessels and their relationships to blood vessels in rabbit Peyer's patches. *Arch. Histol. Cytol.* 53(Suppl):155.

- 15 Westermann, J., Geismar, U., Sponholz, A., Bode, U., Sparshott, S. M. and Bell, E. B. 1997. CD4⁺ T cells of both the naive and the memory phenotype enter rat lymph nodes and Peyer's patches via high endothelial venules: within the tissue their migratory behavior differs. *Eur. J. Immunol.* 27:3174.
- 16 Miura, S., Tsuzuki, Y., Fukumura, D. *et al.* 1995. Intravital demonstration of sequential migration process of lymphocyte subpopulations in rat Peyer's patches. *Gastroenterology* 109:1113.
- 17 Schulz, O. and Pabst, O. 2013. Antigen sampling in the small intestine. *Trends Immunol.* 34:155.
- 18 Merad, M. and Manz, M. G. 2009. Dendritic cell homeostasis. *Blood* 113:3418.
- 19 Tomura, M., Hata, A., Matsuoka, S., *et al.* 2014. Tracking and quantification of dendritic cell migration and antigen trafficking between the skin and lymph nodes. *Sci. Rep.* 4:6030.
- 20 Kawashima, H., Petryniak, B., Hiraoka, N. *et al.* 2005. N-acetylglucosamine-6-O-sulfotransferases 1 and 2 cooperatively control lymphocyte homing through L-selectin ligand biosynthesis in high endothelial venules. *Nat. Immunol.* 6:1096.
- 21 Lee, M., Kiefel, H., LaJevic, M. D. *et al.* 2014. Transcriptional programs of lymphoid tissue capillary and high endothelium reveal control mechanisms for lymphocyte homing. *Nat. Immunol.* 15:982.
- 22 Habtezion, A., Nguyen, L. P., Hadeiba, H. and Butcher, E. C. 2016. Leukocyte trafficking to the small intestine and colon. *Gastroenterology* 150:340.
- 23 Ager, A. 2017. High endothelial venules and other blood vessels: critical regulators of lymphoid organ development and function. *Front. Immunol.* 8:45.
- 24 Moussion, C. and Girard, J. P. 2011. Dendritic cells control lymphocyte entry to lymph nodes through high endothelial venules. *Nature* 479:542.
- 25 Iwasaki, A. and Kelsall, B. L. 2000. Localization of distinct Peyer's patch dendritic cell subsets and their recruitment by chemokines macrophage inflammatory protein (MIP)-3alpha, MIP-3beta, and secondary lymphoid organ chemokine. *J. Exp. Med.* 191:1381.
- 26 Matsuno, K., Ueta, H., Shu, Z. *et al.* 2010. The microstructure of secondary lymphoid organs that support immune cell trafficking. *Arch. Histol. Cytol.* 73:1.
- 27 Zhou, S., Ueta, H., Xu, X. D., Shi, C. and Matsuno, K. 2008. Predominant donor CD103⁺CD8⁺ T cell infiltration into the gut epithelium during acute GvHD: a role of gut lymph nodes. *Int. Immunol.* 20:385.
- 28 Murai, M., Yoneyama, H., Ezaki, T. *et al.* 2003. Peyer's patch is the essential site in initiating murine acute and lethal graft-versus-host reaction. *Nat. Immunol.* 4:154.
- 29 Yu, B., Ueta, H., Kitazawa, Y. *et al.* 2012. Two immunogenic passenger dendritic cell subsets in the rat liver have distinct trafficking patterns and radiosensitivities. *Hepatology* 56:1532.